Journal of Membrane Science 497 (2016) 339–347

Contents lists available at ScienceDirect

Journal of Membrane Science

journal homepage: www.elsevier.com/locate/memsci

Dielectric measurements of fouling of nanofiltration membranes by sparingly soluble salts

Weiliang Hao [a], Man Yang [a], Kongshuang Zhao [a,*], Jiaoning Tang [b]

[a] College of Chemistry, Beijing Normal University, Beijing 100875, China
[b] Shenzhen Key Laboratory of Special Functional Materials, College of Materials Science and Engineering, Shenzhen University, Shenzhen 518060, China

ARTICLE INFO

Article history:
Received 5 May 2015
Received in revised form
16 September 2015
Accepted 19 September 2015
Available online 25 September 2015

Keywords:
Dielectric spectroscopy
Sparingly soluble salt
Nanofiltration membrane
Fouling

ABSTRACT

The dielectric spectroscopy of three industrial nanofiltration (NF) membranes NF90, NF270 and NF-, before and after fouled by $CaCO_3$, $CaSO_4$, $BaSO_4$, $SrSO_4$, were measured. The fouling process and different fouling mode caused by the different membrane pore radius were monitored by dielectric spectroscopy. The NF270 and NF- were mainly fouled in the inner of the membrane pore and NF90 was fouled both in the inner of the membrane pore and on the membrane surface where a scaling layer formed. By analyzing the dependence of dielectric parameters on the fouling time, the relaxation mechanisms of different membrane systems were explained: for the membrane NF270 and NF-, the relaxation observed at the initial stage of fouling process was the result of cooperation of interfacial polarization (between the fouled membrane and deionized water) and the concentration polarization (near the membrane surface) which is from the dissociation of the scale formed by insoluble salts (denoted as CP hereafter), and for that of membrane NF90, in addition to the above two mechanisms, the interfacial polarization between fouling layer and deionized water also contributes. The relaxation after 4 h was mainly controlled by the interfacial polarization between the fouled membrane and solution interface. Further, taking the membrane fouled by $CaSO_4$ as an example, the dielectric analysis was carried out by introducing a constant-phase-element (CPE) to circuit to describe the fouled membrane and the scaling layer. Our finding indicates that the size of membrane pore would influence the fouling process. The feasibility of dielectric spectroscopy as a noninvasive method to monitor the fouling process of internal and surface of membrane was also discussed.

1. Introduction

Nanofiltration (NF) membrane is widely used in drinking water production, water treatment and so on [1]. However, membrane fouling caused by sparingly soluble salt that adhere to pores and the surface of the membrane reduces the membrane separation efficiency, increases costs and shortens membrane life [2]. Therefore, the research on membrane fouling has attracted extensive attention.

Understanding of the micromechanism of membrane fouling is of vital importance to membrane fouling control and cleaning. Although there is no generally accepted theory to explain the complex question, traditionally, the initial decline of membrane flux is attributed to concentration polarization [3], while the long-term decline is attributed to membrane fouling [4]. Despite the mechanisms of concentration polarization and membrane fouling are totally different from each other, the presence of CP phenomenon leads to elevated concentration of solutes and/or particles at the membrane surface and the concentration of these solutes can reach oversaturated easier, which increases the risk of membrane fouling. Hence, it is necessary to take the CP phenomenon into consideration when studying the membrane fouling process.

Up to now, several methods could be used for membrane fouling study, which includes identification of pollutant component and morphology and monitoring the formation process of pollutant. In addition to chemical analytic methods, some characterization techniques, such as scanning electron microscope (SEM) [5], atomic force microscope (AFM) [6], X-ray fluorescence spectrometry (XRF) [7] and so on, could also provide information about pollutant's morphology, structure and elements, etc. However, these off-line techniques could not track the formation process of the pollutant on membrane surface.

Methods for in situ detection of membrane fouling mainly consists of direct observation of particle deposition on membrane

* Corresponding author.
E-mail address: zhaoks@bnu.edu.cn (K. Zhao).

http://dx.doi.org/10.1016/j.memsci.2015.09.042
0376-7388/

surfaces by a microscope [8,9]; in situ observation of the change of particle cake layer using laser technique [10,11]; the processes study of scaling layer formation and particle deposition on membrane surface with ultrasonic time-domain reflectometry (UTDR) [12,13]. However, relatively expensive equipment and complicated operation make these methods above hard to popularize in practice. Meanwhile, some methods for concentration polarization study have also been developed, which mainly consists of shadowgraph [14], Magnetic resonance imaging (MRI) [15], Electron diode array microscope (EDAM) [16], etc. These methods could provide information on solution concentration within the concentration polarization layer and the thickness of concentration polarization layer and so on, however, complicated operation limit their application area.

Electrochemical impedance spectroscopy (EIS) method has also been widely used to study membrane fouling due to its relatively simple experiment equipment. Chilcott et al. [17] and Gaedt et al. [18] proposed its feasibility for investigating membrane fouling, the results indicate that the method has potential for monitoring the deposition of particulate that can lead to fouling. Park et al. [19] investigated bovine serum albumin (BSA) fouling of the cation-exchange membrane and anion-exchange membrane using impedance spectroscopy. Differences in the dispersions arising from fouling were identified by subtracting the impedance of the solution from those of unfouled and fouled IEMs in solution. They also [20] studied the fouling phenomena of an anion-exchange membrane by BSA using the current–voltage (*I*–*V*) relation and electrical impedance spectroscopy. Two distinguishable slopes were observed in the over-limiting current density(LCD) region of *I*–*V* curve, indicating the change of resistance was caused by the structure changes of the BSA fouling layer formed on membrane surface. Lee et al. [21] investigated ion exchange membrane fouling by sodium dodecylbenzenesulfonate (SDBS). The equivalent circuits show that an additional layer formed on the membrane surface, increasing the electrical resistance to permeation of ions through the membrane. Kavanagh [22] analyzed the electrical property change of reverse osmosis membrane before and after fouled by $CaCO_3$ using the equivalent circuit and found that fouling could potentially be measured by the increased impedance at frequencies below 100 Hz. Moreover, electrochemical impedance spectroscopy could also be used to study concentration polarization. Zhao et al. [23,24] investigated the concentration polarization phenomena in ion-exchange membrane/solution system under application of d.c. bias voltage, the conductivity of the reduced ion concentration and the thickness of the concentration polarization layer were obtained by modeling analysis. Sang et al. [25] discussed the formation and structure of concentration polarization layer (CPL) on ion-exchange membrane-solution interface under high frequency AC electrical field, and investigated the relations of CPL thickness with the electrolyte concentration and ion-exchange membrane property. In recent years, Antony et al. [26] studied the fouling of reverse osmosis membrane during the filtration of water containing $CaCO_3$. They found that dielectric structural modeling was able to detect and characterize five electrically distinct layers and a concentration/diffusion polarization. Sim et al. [27] used Silica and BSA as model foulants, and studied the fouling process of single and binary foulants on the reverse osmosis (RO) membrane by EIS. Hu et al. [28] used EIS to measure the electrical properties changes during calcium sulfate scaling in a reverse osmosis system. They found that the conductance signal of 10–100 Hz can signal the nascent stages of scale formation. Cen et al. [29] detect the fouling of reverse osmosis membranes, during filtration of industrial (molasses) waste water and model feeds containing silica and BSA foulants. They found that the low frequency (1 Hz) capacitance was the most sensitive measurement and was more sensitive than either conductance or fluxdecline.

From the reviews above, we can see that the studies about membrane fouling and concentration polarization using electrochemical impedance spectroscopy were mainly focused on the systems of ion-exchange membrane/solution and reverse osmosis membrane, and few researches on the nanofiltration membrane fouling and the accompanying concentration polarization phenomenon.

In the present work, the fouling process of three types of nanofiltration membrane (NF90, NF-, NF270) fouled by $CaCO_3$, $CaSO_4$, $BaSO_4$, $SrSO_4$ solutions was simulated in the laboratory. Dielectric measurements for the three nanofiltration membranes fouled at different time were carried out over a frequency range from 40 Hz to 11 MHz. The dielectric parameters and phase parameters of membranes were obtained by dielectric analysis. By analyzing the dependence of these parameters on the fouling time, the feasibility of dielectric spectra for monitoring NF fouling and concentration polarization caused by sparingly soluble salt was assessed.

2. Experiment and materials

2.1. Chemicals and membranes

Na_2CO_3, $CaCl_2$, $BaSO_4$ and $SrSO_4$ were analytical grade and $CaSO_4 \cdot 2H_2O$ was chemical grade. Deionized water (D.W.) was used in the experiment. Three commercial NF membranes (Dow, USA), NF90, NF270 and NF-, were used. Some parameters of the membranes are shown in Table 1.

2.2. Preparation of scaling solution

2.2.1. Preparation of saturated $CaCO_3$ solution

Solutions of Na_2CO_3 and $CaCl_2$ having the same concentration (6 mM) were mixed fully with a volume ratio of 1:1. After standing for some time, the supernatant fluid was used as the scaling solution.

2.2.2. Preparation of saturated $CaSO_4$ solution

The $CaSO_4$ powder was dissolved directly in deionized water and the supernatant fluid was used as scaling solution. The preparation methods of $BaSO_4$ and $SrSO_4$ solution are the same as $CaSO_4$ solution.

2.3. Simulation of membrane fouling and dielectric measurements

The experiment is divided into two stages. The first stage is to simulate the fouling process of nanofiltration membrane and the second stage is to carry out dielectric measurements for the fouled membrane.

2.3.1. Experiment of membrane fouling

The experimental set-up for membrane fouling is shown in Fig. 1. The membrane fouling experiment is a single channel cross-flow filtration process. The NF membrane is fixed in the middle of a rectangular cell with a cylinder chamber, separating the cylinder chamber into two chambers. The effective surface area of the membrane is actually the bottom area of the cylinder. The scaling solution was pumped from a stirred tank using peristaltic pump to the rectangular cell, flowing along the active layer of NF membrane, and then recycled back to the stirred tank. During filtration, as crystals would deposit at the membrane surface, saturated feed solution was added into stirred tank to ensure the feed concentration was constant. Flow pressure and temperature were kept at 0.055–0.075 MPa and 20 ± 1 °C, respectively.

Table 1
Material characteristics of three nanofiltration membranes [30].

Membrane	NF90	NF270	NF-
Material	Polyamide	Polyamide	Polypiperazineamide
pore radius r_p (nm)	0.294	0.364	0.368

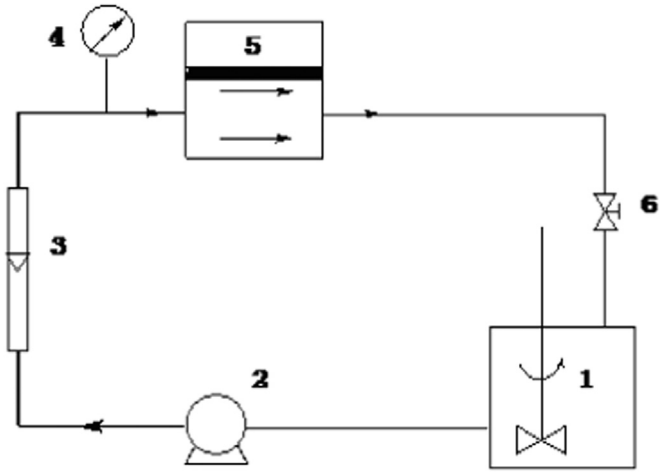

Fig. 1. Scheme of experiment apparatus for membrane fouling. (1) Stirred tank (2) peristaltic pump (3) liquid flowmeter (4) pressure gauge (5) NF membrane (6) pressure valve.

2.3.2. Dielectric measurements

Dielectric measurements were performed with an Agilent 4294A Precision Impedance. The measuring cell [31] consists of a pair of platinum disk electrodes whose area S is 3.14 cm^2. The cell constant S/L is measured to be 2.6 cm (L is the distance between the two electrodes). A specimen membrane separated the cylindrical compartments between the electrodes, and the two compartments were filled with D.W.. In other words, the nanofiltration membrane used in this work is sandwiched between two aqueous solution phases to form a D.W./membrane/ D.W. system. The capacitance C and conductance G of these systems were measured over the frequency range from 40 Hz to 11 MHz.

The dielectric measurements of D.W./clean membrane/D.W. system was carried out as a contrast before the membrane fouling experiment. During the fouling experiment, the membrane would be taken out from the circulating device every two hours, and then put into the measuring cell immediately, to perform the dielectric measurement on the system of D.W./fouled membrane/ D.W.. After that, the membrane would be reloaded to the circulating device for fouling. The total fouling time for each membrane was 14 h, and the time for each dielectric measurement was 30 s.

3. Results and discussions

3.1. Dielectric behavior of different membrane/D.W. system

Fig. 2 shows the dielectric spectroscopy of the membranes NF90, NF270, before (0 h) and after (2–14 h) fouled by $CaSO_4$ and the dielectric spectroscopy when there is no membrane present (D.W.). The dielectric spectroscopy of other three sparingly soluble salts are similar to $CaSO_4$. As indicated in Fig. 2, the fouling process is well detected by dielectric spectroscopy: For NF270 membrane/ D.W. system (Fig. 2a) (membrane NF- is similar to NF270), relaxation strength increases and dielectric relaxation shifts to higher frequency (about 10^5 Hz) after the membrane was fouled; for the NF90 membrane (Fig. 2b), whose pore radius is smaller than NF270, there is only one relaxation appearing at low frequency (about 10^3 Hz) for the unfouled system (0 h), and a new relaxation appears at high frequency (about 10^5 Hz) for the fouled one (2–14 h). The different dielectric behavior of NF270 and NF 90 systems indicates that pore radius plays an important role in fouling process.

Besides, it is noteworthy that for the three unfouled NF membrane, there is only one relaxation was detected, and this relaxation is from the interface between the membrane and water. This result indicates that despite the NF membrane has different layers, heterogeneity of membrane does not cause the interface polarization relaxation. That is say, in the subsequent analysis process, the membrane should be taken as a whole phase.

3.2. Dependence of dielectric increment of system on fouling time

As can be seen from Section 3.1, the fouling mainly caused the changes of relaxation strength of NF- and NF270 as well as the high-frequency relaxation of NF90. Therefore, time dependences of dielectric increment (ΔC) of NF-, NF270 and high frequency relaxation of NF90 were compared in Fig. 3. It is worth noting that the main graph of Fig. 3 is from Fig. 2(a), and the inset is from the high-frequency relaxation of Fig. 2b. Dependences of ΔC on fouling time for the two membranes NF270 and NF- system are similar: ΔC increases distinctly within 2 h, decreases rapidly after 4 h, and in the following 4–14 h increases regularly with the fouling time. Generally, when there is a flux through the membrane, the concentration polarization arises and leads to concentrations of some salts exceed their solubility product and a scale will form. A clear relaxation of concentration polarization will occurs at very low

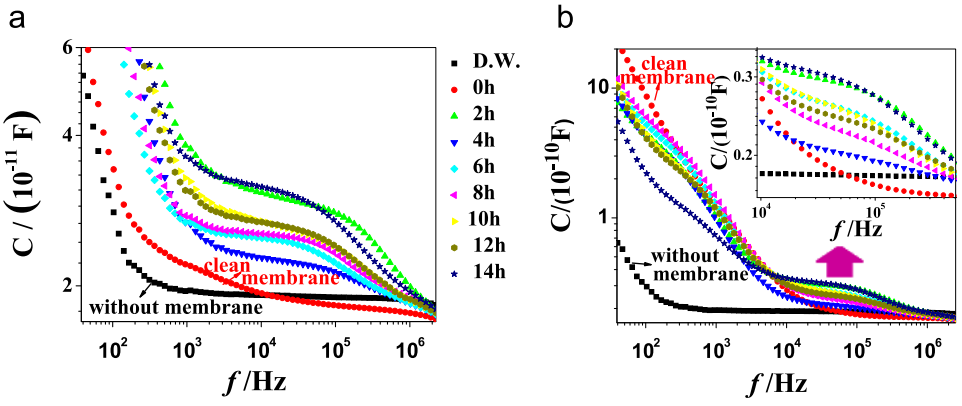

Fig. 2. Frequency dependence of capacitance for the NF270 (a), NF90 (b) before (0 h) and after (2–14 h) fouled by $CaSO_4$ in deionized water at different fouling time. The black solid square (D.W.) is the dielectric spectroscopy when there is no membrane present. The inset in Fig. 2b is an enlarged view of high-frequency relaxation.

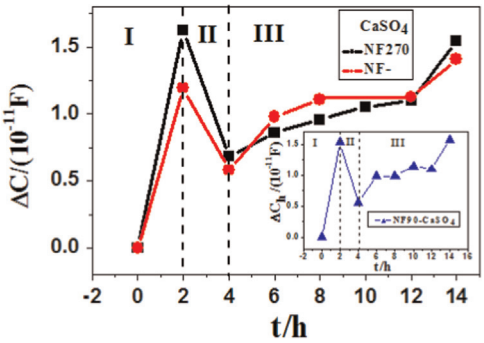

Fig. 3. Dependences of dielectric increment (ΔC) of NF270 and NF- systems (fouled by $CaSO_4$) and high-frequency dielectric increment ΔC_h of NF90 system on the fouling time.

frequency, as studied by some researchers [26–28,32]. While without the presence of flux, the dissociation of the scale formed by insoluble salts will forms a concentration polarization layer with a conductivity distribution and the location of the relaxation may shift to higher frequency. This was detected by our previous theoretical [33] and experimental work [23,24] and other researchers [34]. However, it is important to note that the concentration polarization in this work is from the dissociation of insoluble salts, which is different from the original concentration polarization layer when there is a flux. According to the report [35] that the capacitance value of the membrane/solution system is proportional to the insoluble salt concentration near the membrane pore, and the fact that dielectric increment (ΔC) is proportional to the capacitance value of the system in this work, we infer that initial increment of the capacitance (stage) was mainly due to the CP, which was caused by the partial dissociation of insoluble salt nuclei near the membrane pore; the reason for the subsequent decrease of the capacitance (stage) was that salt nuclei grown beyond the critical size and became more stable and can hardly to redissolve [36], which leads to the decline of the CP. The relaxation before 4 h was the result of cooperation of CP (near the membrane surface) and the interfacial polarization (between the membrane and deionized water); the relaxation before 2 h was mainly controlled by the CP. As the character frequency of the CP and interfacial polarization are close to each other, only the relaxation strength changed with time (This will be demonstrated below), while the relaxation number remained unchanged. In stage , the contribution of CP to relaxation could be neglected [37], and the relaxation was mainly controlled by the interfacial polarization. Comparing the main graph and inset of Fig. 3, it is obvious that the changing trend of dielectric increment for the three membranes is consistent. But it is worth noting that only one relaxation was observed for NF270 and NF- of the main graph, and the capacitance increment is from this relaxation. While for NF90, two relaxations were observed and the inset is the result of high-frequency relaxation. This means that, compared with NF- and NF270, there is an additional low-frequency relaxation in the NF90 system, and this is caused by different fouling mechanisms. For the membrane NF90, the CP also exists. The difference is that due to a smaller pore size of membrane NF90, the insoluble salts are more likely to accumulate on the membrane surface, so CP is mainly from the dissociation of the fouling layer in water, which is different from that of membrane NF270 and NF-. In addition, it's important to note that the high-frequency relaxation of this system is composed of concentration polarization and interfacial polarization between fouling layer and water, and the characteristic frequency of them are similar.

To confirm the inference that the relaxation is caused by both concentration polarization and interfacial polarization and their characteristic frequencies are close to each other, we applied the method given by Zhao et al. [23] to fit the experimental data of capacitance C, and to separate these two effects. The equations used for fitting are as follows:

The complex capacitance of the whole system C^* can be expressed by:

$$\frac{1}{C^*} = \frac{1}{C_p^*} + \frac{1}{C_m^*} + \frac{1}{C_w^*} \tag{1}$$

where C_p^*, C_m^* and C_w^* are complex capacitance of CP layer, the nanofiltration membrane and D.W., respectively. The complex capacitance C^* of each component is defined as:

$$C^* = C - jC'' = C + \frac{G}{j2\pi f} \tag{2}$$

The conductance G_p and capacitance C_p of the CPL can be expressed by:

$$C_p(f) = \frac{S(\kappa_2 - \kappa_1)}{d_{CPL}} \frac{B/\omega}{A^2 + B^2} \tag{3a}$$

$$G_p(f) = \frac{S(\kappa_2 - \kappa_1)}{d_{CPL}} \frac{A}{A^2 + B^2} \tag{3b}$$

where S is effective area of CP layer, which is also the effective area of the membrane. d_{CPL} refers to the thickness of CP layer. $\omega(=2\pi f)$ is angular frequency of the applied ac electric field, κ_1 and κ_2 are the conductivity at both sides of the CPL. A and B are functions of κ_1 and κ_2, as expressed by:

$$A = \frac{1}{2} \ln\left(1 + \frac{(\frac{\kappa_2}{\kappa_1})^2 - 1}{1 + (\frac{\varepsilon_w \varepsilon_0}{\kappa_1})^2 \omega^2}\right) \tag{4a}$$

$$B = \tan^{-1} \frac{(\kappa_2 - \kappa_1)\omega\varepsilon_w\varepsilon_0}{(\omega\varepsilon_w\varepsilon_0)^2 + \kappa_2\kappa_1} \tag{4b}$$

where $\varepsilon_0(=8.8542 \times 10^{-12}\ \mathrm{F\ m^{-1}})$ is vacuum permittivity, ε_w is relative permittivity of CPL as well as that of bulk scaling solution.

Taking the fitting results of NF270-$CaSO_4$ system (t=2 h) as an example, as indicated in Fig. 4, the spectra calculated by the fitting procedure are in good agreement with the experimental data (hollow circles). When $\kappa_1 = \kappa_2$ and the other values remained unchanged, the CP contribution would be removed from the whole system, and only the relaxation caused by interfacial polarization could be observed, as is shown by the broken blue line. It is clear from this figure that because of the removal of CP the relaxation

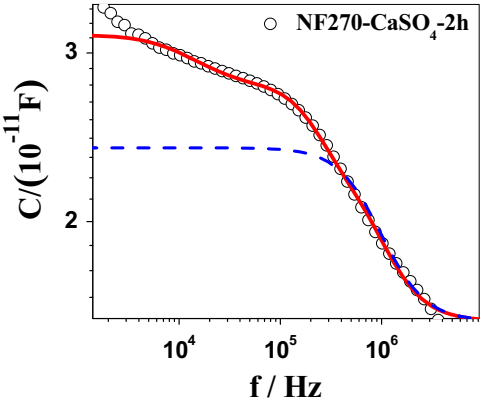

Fig. 4. Frequency dependence of capacitance for the system of NF270/D.W. (fouled by $CaSO_4$ at t=2 h).

strength decreased, and the character frequency of CP and interfacial polarization are close to each other (about 10^5–10^6 Hz). Therefore, the speculation for the relaxation mechanism is reasonable.

The hollow circles represent the experimental data; the straight line is the fitting line obtained by three phase dielectric model; the dashed line is obtained by simulation when $\kappa_1 = \kappa_2$.

The above shows that the changing trend of CP and the membrane fouling microprocess can be obtained indirectly by tracking the time dependence of capacitance of these systems.

3.3. Analysis of membrane fouling mechanisms

The above analysis shows that the difference of relaxation mode in different NF systems was related to the value of the membrane pore size. For membrane NF270, whose pore size is relatively larger, most of the crystal particles, $CaSO_4$, entered into the inner of the membrane pores and few particles deposited on the membrane surface. Hence, the dominant fouling mechanism of membrane NF270 was internal fouling, which just leads to the change of the structural and electrical properties of the membrane phase, so, the interfacial property changed. Besides, considering the contribution of CP to the relaxation, the relaxation strength also changed. For the membrane NF90, whose pore size is relatively smaller, only few particles entered into the membrane pores and blocked the pores blockage quickly, and then plenty of particles deposited on the membrane surface, where a scaling layer formed (external fouling). The properties of the newly formed scaling layer and the fouled membrane were totally different, in addition, CP (which was not obvious for the system) also contributed to the relaxation mechanism. So, a new relaxation, which was mainly caused by interfacial relaxation, appeared. The membrane/scaling layer/D.W. system contains two interfaces with different properties. Therefore, the measuring result shows double relaxations as shown in Fig. 2b, which can be predicted by interface polarization theory [38]. Fig. 5 shows the formation of internal fouling (a), pore blockage (b) and external fouling (c) of membrane and the schematic for the two phase systems composed of NF270 (or NF-) and deionized water and three phase systems composed of deionized water, fouling layer and NF90 membrane.

3.4. Determination of phase parameters

3.4.1. Electrical circuit model

The electrical circuit model method was used to analysis the data, and to obtain further information about the fouled membrane and the scaling layer. Because the interface between the support layer and effective layer did not be detected in Fig. 2, the NF membrane is taken as a whole membrane phase. At the same time, considering that the characteristic frequency for the CP and interfacial polarization are similar, and CP has no contribution to the number of relaxation. Therefore, for convenience, we consider CP phase and membrane phase to be a whole phase for membranes NF270 and NF-, and take CP phase and fouling layer phase as a whole phase for the membrane NF90.

The two-phase system (membrane phase and aqueous phase) in Fig. 5a and three-phase system (the membrane phase, the aqueous phase and fouling layer) in Fig. 5c can be represented by the equivalent circuit model of Fig. 6: to simulate a bilamellar structure composed of membrane NF270 (NF-) and D.W. (Fig. 6a), and the ternary system composed of fouling layer, membrane NF90 and D.W. (Fig. 6b), respectively. For a membrane or layer with porosity or non-uniform thickness, their behavior can be described by constant phase element instead of simple elements such as ideal capacitances or resistances [39–43]. In this work, constant phase elements (CPE) are used to describe the capacitive properties of the membrane and the fouling layer [44]. Whichever electrical circuit model is used, the dielectric measurement can be considered as the frequency dependence of complex capacitance $C(f)$ of the whole system (Fig. 6c), which is equivalent to the more usual approach in terms of Maxwell–Wagner elements each consisting of a parallel combination of a resistance and capacitance.

Complex capacitances of the two-phase and three-phase systems are represented by Eq. (5a) and Eq. (5b), respectively:

$$\frac{1}{C_{\text{two}}^*} = \frac{1}{C_{\text{m}}^*} + \frac{1}{C_{\text{w}}^*} \tag{5a}$$

$$\frac{1}{C_{\text{three}}^*} = \frac{1}{C_{\text{m}}^*} + \frac{1}{C_{\text{f}}^*} + \frac{1}{C_{\text{w}}^*} \tag{5b}$$

where $C_{\text{two(three)}}^*$ C_{m}^* C_{f}^* and C_{w}^* are the complex capacitance of the whole system, membrane, fouling layer and D.W., respectively. Complex capacitances are defined as:

$$C_{\text{two(three)}}^* = C_{\text{two(three)}} + \frac{G_{\text{two(three)}}}{j2\pi f} \tag{6a}$$

$$C_{\text{w}}^* = C_{\text{w}} + \frac{G_{\text{w}}}{j2\pi f} \tag{6b}$$

$$C_{\text{m}}^* = Q_{\text{m}} + \frac{G_{\text{m}}}{j2\pi f} \tag{6c}$$

$$C_{\text{f}}^* = Q_{\text{f}} + \frac{G_{\text{f}}}{j2\pi f} \tag{6d}$$

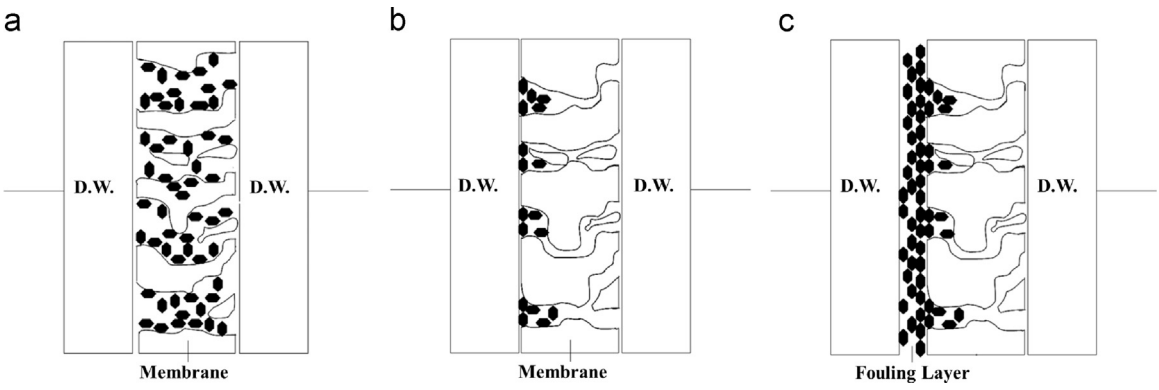

Fig. 5. The formation of internal fouling (a), pore blockage (b) and external fouling (c) of nanofiltration membrane and the schematic for the two phase systems composed of NF270 (or NF-) and deionized water (a) and three phase systems composed of deionized water, fouling layer and NF90 membrane (c).

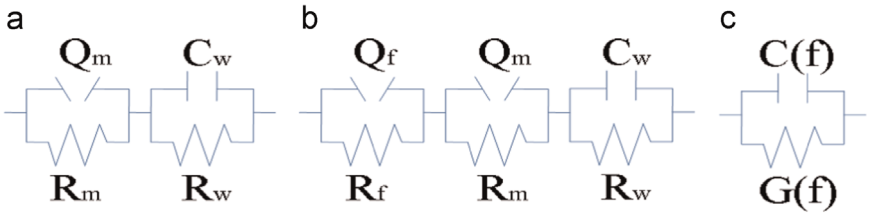

Fig. 6. The circuit models to simulate a bilamellar structure composed of membrane and D.W. (a) and fouling layer, membrane and D.W. (b), and equivalent capacitance $C(f)$ and conductance $G(f)$ for the whole system (c).

The admittance of a CPE is given by:

$$Q_m(f) = Y_0(j2\pi f)^n \tag{7}$$

where Y_0 ($\Omega\ s^{-n}$) and n are two empirical parameters. When $n=1$, 0.5, 0, −1, the CPE is called pure capacitance, Warburg impedance, pure resistance and inductance, respectively. The true capacitance value of the CPE can be expressed as [45]:

$$C = Y_o(\omega''_m)^{n-1} \tag{8}$$

where ω''_m is the frequency at which the imaginary component of impedance reaches the maximum.

3.4.2. Phase parameters of biphase system: fouling of membranes NF270 and NF-

By Eq. (5a), the curve-fitting was carried out on the systems of NF270 (NF-), before and after fouled by insoluble salt and then the phase parameters of the membrane and D.W. were obtained by Eq. (8). We take the fitting results of system NF270-CaSO4 as example (Table 2). As the parameters change of water phase is tiny, it is not listed here and the discussion is mainly focused on the capacitance and resistance of membrane, which are obtained by using formula (5)–(7) and equivalent circuit model to fit the experimental data.

Fig. 7a shows the dependence of membrane capacitance C_m for the system of NF270-$CaSO_4$ on fouling time. It can be seen that membrane capacitance decreased rapidly after being fouled, which was mainly due to the pore blocking. This change can be explained qualitatively by Eq. (9):

$$\varepsilon_m = \varepsilon_w f_w + \varepsilon_m' f_m' + \varepsilon_{salt}(1 - f_w - f_m') \tag{9}$$

where ε_m is the permittivity of the whole membrane phase, ε_w is the permittivity of water (about 80 at 20 °C), ε_m' is the permittivity of dry membrane (3–4), ε_{salt} is the permittivity of insoluble salt (the permittivity of $CaSO_4$ is 5.6), f_w, f_m' are the volume fraction of water and pure membrane matrix in the whole membrane phase, respectively, and $1 - f_w - f_m'$ is the volume fraction of insoluble salt (in the pore of membrane) in the whole membrane phase.

Before fouled by insoluble salt, the membrane phase was composed of membrane matrix and water in the membrane pores; after the insoluble salt crystal particles entered into the membrane pores, the volume fraction of water f_w decreased. Because the permittivity of insoluble salt is much smaller than that of water, the permittivity of the whole membrane phase ε_m decreased, which leads to the decrease of the membrane capacitance.

Table 2
Parameters of NF270 membrane fouled by $CaSO_4$ at different fouling times.

t/h	$C_m/(10^{-17}F)$	$R_m(=1/G_m)/(10^4\ \Omega)$
0	12635	0.17381
2	1.1547	1.1421
4	4.2978	3.1415
6	3.8848	4.3459
8	4.1584	2.9260
10	3.6945	3.7319
12	3.2091	2.8603
14	2.0354	3.2373

As shown in Fig. 7a, the value of the membrane capacitance reaches the minimum at the initial stage ($t=2$ h) of fouling process. This was because that: on one hand, the membrane pore had been partially blocked by crystal particles and the permittivity of the membrane phase decreased after 2 h; on the other hand, most of the insoluble salt molecules existed in the form of crystal nuclei, which are very small [36] and can easily attach to membrane surface to block the membrane pore. When conducting dielectric measurement, the small crystal nuclei can redissolve into water, leading to concentration polarization. The two effects cause the sharp drop of membrane capacitance at 2 h. When the crystal nuclei grown bigger enough, they cannot attach to membrane surface easily any longer and subsequently some of them would drop off from the membrane surface. Therefore, the value of membrane capacitance C_m increases at 4 h. After that, the value of membrane capacitance C_m decreased slowly with time, which was mainly due to the increasing degree of membrane blocking. Fig.7b shows that membrane resistance R_m increases at the first 6 h. This was due to the pore blocking (the ions is difficult to go through the membrane). And then R_m fluctuated in a certain range, which probably means that the pore blocking has reached to a equilibrium.

The above analysis show that the fouling process of membrane NF270 (NF-) was monitored by the variation of membrane capacitance with fouling time. It also illustrates that the concentration polarization does exist in fouling process. In addition, the rationality of taking the concentration polarization and membrane phase as a whole phase is also demonstrated.

3.4.3. Phase parameters of three-phase system: the fouling of membranes NF90

Eq. (5a) was used to fit the unfouled membrane system and Eq. (5b) was used to fit the fouled membrane system. The parameters of membrane and fouling layer of the three-phase circuit model in Fig. 6b were obtained by Eq. (8). We take the fitting results of NF90-$CaSO_4$ as an example.

Fig. 8 shows that membrane capacitance C_m decreases and membrane resistance R_m increases with fouling time, respectively, indicating an increasing degree of membrane blocking. Moreover, membrane capacitance C_m of NF90 did not show the minimum at $t=2$ h, as NF270. The difference may be caused by the influence of scaling layer on the membrane fouling.

The scaling layer can be considered as a plate capacitor and the C_f change with time can be explained by Eq. (10) as follows:

$$C_f = \varepsilon_f \varepsilon_0 \frac{S_f}{d_f} \tag{10}$$

where C_f is the capacitance of scaling layer, ε_f is permittivity of scaling layer phase, S_f is the area of scaling layer, d_f is the thickness of scaling layer.

The rapid increase at $t=2$–4 h of C_f in Fig. 9a indicates that, at the initial stage of membrane fouling the area of scaling layer S_f increased with time, while the thickness of scaling layer d_f remained unchanged. The accompanying decrease of R_f (Fig. 9b)

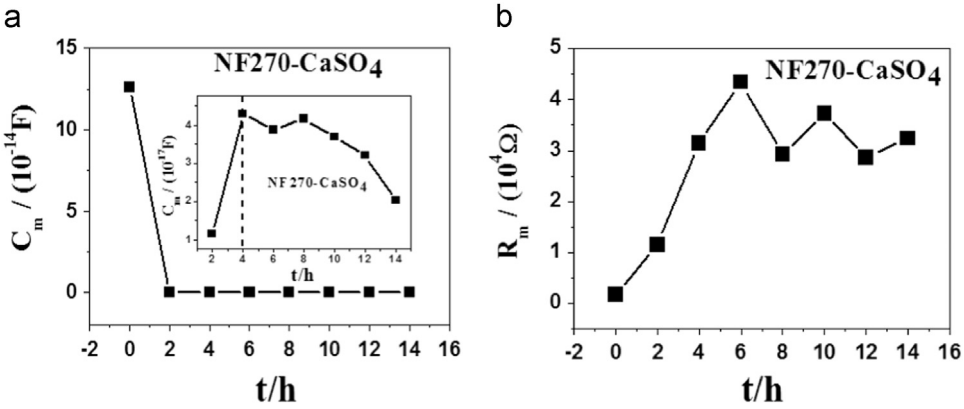

Fig. 7. Dependence of membrane capacitance C_m (a) and membrane resistance R_m (b) for the system of NF270-$CaSO_4$ on fouling time.

indicates a decreasing ion concentration in fouling layer because of the reduced CP. The decrease of C_f at t=4–10 h suggest that the thickness of scaling layer d_f is increased with time, while the area of scaling layer S_f remained unchanged; while the increase of C_f after 10 h suggests that as the fouling process goes on, the particles deposited on membrane surface would be pressed by the newly deposited particles, leading to the decrease in the thickness of scaling layer. The reason for the change of R_f during 4–14 h was the same to C_f.

The above discussion demonstrates that it is reasonable to consider the CP and fouling layer as one phase and the CP is indeed generated from the dissociation of fouling layer in water.

3.4.4. Influence of insoluble salt properties on fouling process of membrane

The fouling processes of NF90 membrane by four different insoluble salts were compared (Fig. 10) and different dependence of C_f on fouling time for the four insoluble salts may suggest their different crystallization mechanisms.

4. Conclusions

Dielectric measurements for nanofiltration membranes NF90, NF270 and NF-, before and after fouled by $CaCO_3$, $CaSO_4$, $BaSO_4$, $SrSO_4$, were conducted. The dielectric spectroscopy of three NF membranes shows two totally different relaxation modes. The difference in relaxation modes was explained reasonably by analyzing the time dependence of capacitance. In addition, the modeling analysis indicates that the membrane pores size could influence the fouling processes of nanofiltration membrane.

Although the research approach, applied in the present study, for membrane fouling processes is quasi monitoring, the time dependence of capacitance of membrane/solution system indicates that dielectric spectra has huge potential on monitoring membrane fouling in a noninvasive way and can also probably provide us with useful information about the qualitative distinguishment of membrane pore size and crystallization mechanisms of insoluble salt. However, this method is incapable of accurate quantification due to the inhomogeneous thickness of crystalline substance, which indicates that this method may be more suitable for monitoring fouling by organic and other non-crystalline substances.

Acknowledgments

Financial support of this work by the National Natural Scientific Foundation of China (No. 21173025 and 21473012), the National High Technology Research and Development Program of China (863 Program, 2012AA030312) and the Major Research Plan of NSFC (No. 21233003) are gratefully acknowledged.

List of Symbols

C	total measured capacitance (F)
ΔC	dielectric increment (F)
C^*	complex capacitance total measured capacitance (F)
C_f^*	capacitance of fouling layer (F)
C_p^*	complex capacitance of concentration polarization

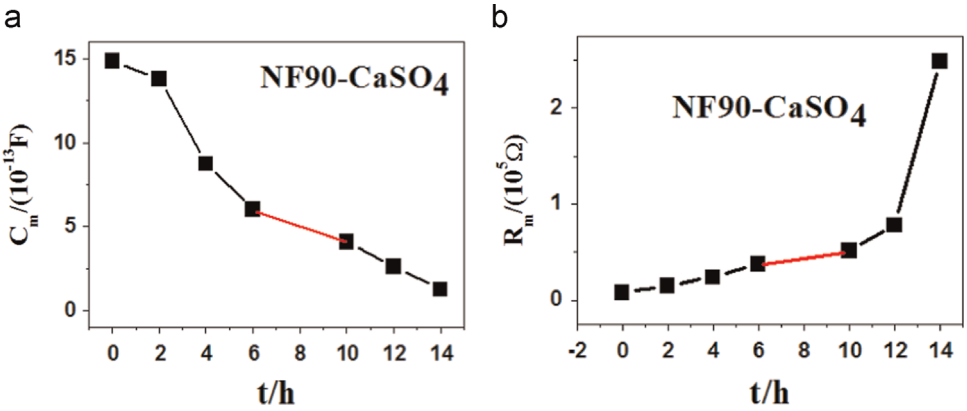

Fig. 8. Dependence of membrane capacitance C_m (a) and membrane resistance R_m (b) for the system of NF90-$CaSO_4$ on fouling time.

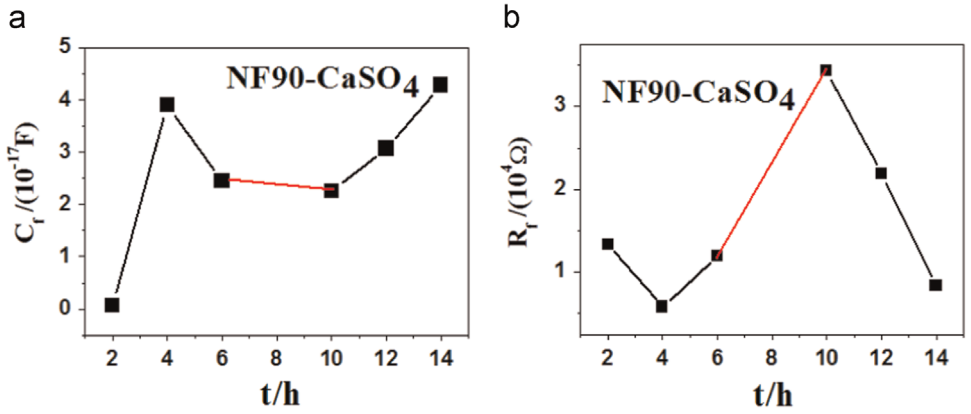

Fig. 9. Dependence of capacitance C_f (a) and resistance capacitance R_f (b) of scaling layer for the system of NF90-$CaSO_4$ on fouling time.

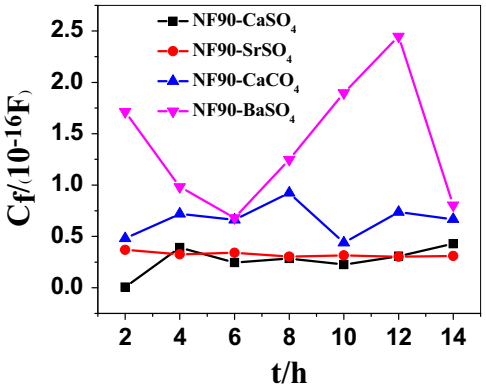

Fig. 10. Dependence of scaling layer capacitance C_f of membrane NF90 for the four insoluble salts on fouling time.

	layer (F)
C_m^*	complex capacitance of nanofiltration membrane (F)
C_w^*	complex capacitance of water phase (F)
G	total measured conductance (S)
G_p	conductance of concentration polarization layer (S)
$Q_{m(f)}$	constant phase elements
R_m	resistance of membrane (Ω)
R_f	resistance of fouling layer (Ω)
R_w	resistance of concentration polarization layer as well as bulk scaling solution (Ω)
Y_0, n	empirical parameters
ε_0	permittivity of vacuum ($=8.8541 \times 10^{-12}$ Fm^{-1})
ε_w	permittivity of concentration polarization layer as well as bulk scaling solution
ε_m	permittivity of the whole membrane phase
ε'_m	permittivity of dry membrane
ε_{salt}	permittivity of insoluble salt
ε_f	permittivity of scaling layer phase
f_w	volume fraction of water in the whole membrane phase
f_m'	volume fraction of pure membrane matrix in the whole membrane phase
f	measuring frequency (Hz)
j	unit imaginary
ω	angular frequency of the applied ac electric field (rad/s)
ω''_m	angular frequency where imaginary component of impedance reaches the maximum (rad/s)
κ_1, κ_2	conductivity at both sides of concentration polarization layer
A, B	functions of κ_1 and κ_2
S	effective area of membrane (m^2)
S_f	area of scaling layer (m^2)
L	distance between the two electrodes (m)
d_{CPL}	thickness of CPL (m)
d_f	thickness of scaling layer (m)

References

[1] A.S. Al-Amoudi, Factors affecting natural organic matter (nom) and scaling fouling in Nf membranes: a review, Desalination 259 (2010) 1–10.
[2] S. Shirazi, C.-J. Lin, D. Chen, Inorganic fouling of pressure-driven membrane processes—a critical review, Desalination 250 (2010) 236–248.
[3] J.C. Chen, Q. Li, M. Elimelech, In situ monitoring techniques for concentration polarization and fouling phenomena in membrane filtration, Adv. Colloid Interface Sci. 107 (2004) 83–108.
[4] L. Song, Flux decline in crossflow microfiltration and ultrafiltration: mechanisms and modeling of membrane fouling, J. Membr. Sci. 139 (1998) 183–200.
[5] C. Tzotzi, T. Pahiadaki, S. Yiantsios, A. Karabelas, N. Andritsos, A study of Caco 3 scale formation and inhibition in Ro and Nf membrane processes, J. Membr. Sci. 296 (2007) 171–184.
[6] A. Al-Amoudi, R.W. Lovitt, Fouling strategies and the cleaning system of Nf membranes and factors affecting cleaning efficiency, J. Membr. Sci. 303 (2007) 4–28.
[7] N. Her, G. Amy, C. Jarusutthirak, Seasonal variations of nanofiltration (Nf) foulants: identification and control, Desalination 132 (2000) 143–160.
[8] H. Li, A. Fane, H. Coster, S. Vigneswaran, Direct observation of particle deposition on the membrane surface during crossflow microfiltration, J. Membr. Sci. 149 (1998) 83–97.
[9] W.D. Mores, R.H. Davis, Direct visual observation of yeast deposition and removal during microfiltration, J. Membr. Sci. 189 (2001) 217–230.
[10] J. Altmann, S. Ripperger, Particle deposition and layer formation at the crossflow microfiltration, J. Membr. Sci. 124 (1997) 119–128.
[11] M. Hamachi, M. Mietton-Peuchot, Cake thickness measurement with an optical laser sensor, Chem. Eng. Res. Des. 79 (2001) 151–155.
[12] A.P. Mairal, A.R. Greenberg, W.B. Krantz, L.J. Bond, Real-time measurement of inorganic fouling of ro desalination membranes using ultrasonic time-domain reflectometry, J. Membr. Sci. 159 (1999) 185–196.
[13] J. Li, J. Liu, T. Yang, C. Xiao, Quantitative study of the effect of electromagnetic field on scale deposition on nanofiltration membranes via Utdr, Water Res. 41 (2007) 4595–4610.
[14] V. Vilker, C. Colton, K. Smith, Concentration polarization in protein ultrafiltration, Aiche J. 27 (1981) 632–645.
[15] S. Yao, M. Costello, A. Fane, J. Pope, Non-invasive observation of flow profiles and polarisation layers in hollow fibre membrane filtration modules using Nmr micro-imaging, J. Membr. Sci. 99 (1995) 207–216.
[16] R. Mc Donogh, H. Bauser, N. Stroh, U. Grauschopf, Experimental in situ measurement of concentration polarisation during ultra-and micro-filtration of bovine serum albumin and dextran blue solutions, J. Membr. Sci. 104 (1995) 51–63.
[17] T. Chilcott, M. Chan, L. Gaedt, T. Nantawisarakul, A. Fane, H. Coster, Electrical impedance spectroscopy characterisation of conducting membranes: I. theory, J. Membr. Sci. 195 (2002) 153–167.
[18] L. Gaedt, T. Chilcott, M. Chan, T. Nantawisarakul, A. Fane, H. Coster, Electrical impedance spectroscopy characterisation of conducting membranes: Ii. experimental, J. Membr. Sci. 195 (2002) 169–180.

[19] J.-S. Park, T. Chilcott, H. Coster, S.-H. Moon, Characterization of bsa-fouling of ion-exchange membrane systems using a subtraction technique for lumped data, J. Membr. Sci. 246 (2005) 137–144.
[20] J.-S. Park, J.-H. Choi, K.-H. Yeon, S.-H. Moon, An approach to fouling characterization of an ion-exchange membrane using current–voltage relation and electrical impedance spectroscopy, J. Colloid Interface Sci. 294 (2006) 129–138.
[21] H.-J. Lee, M.-K. Hong, S.-D. Han, J. Shim, S.-H. Moon, Analysis of fouling potential in the electrodialysis process in the presence of an anionic surfactant foulant, J. Membr. Sci. 325 (2008) 719–726.
[22] J. Kavanagh, S. Hussain, T. Chilcott, H. Coster, Fouling of reverse osmosis membranes using electrical impedance spectroscopy: measurements and simulations, Desalination 236 (2009) 187–193.
[23] K. Zhao, M. Yasuhiro, K. Asaka, K. Asami, T. Hanai, Dielectric analysis of concentration polarization phenomena at cation-exchange membrane/solution interfaces by frequency variation and dc bias application, J. Membr. Sci. 64 (1991) 163–172.
[24] K. Zhao, K. Asaka, K. Asami, T. Hanai, Dielectric analysis of concentration polarization structure at anion-exchange membrane/solution interface under Dc bias voltage application, J. Colloid Interface Sci. 153 (1992) 562–571.
[25] S. Sang, Q. Wu, K. Huang, A discussion on ion conductivity at cation exchange membrane/solution interface, Colloids Surf. A: Physicochem. Eng. Asp. 320 (2008) 43–48.
[26] A. Antony, T. Chilcott, H. Coster, G. Leslie, In situ structural and functional characterization of reverse osmosis membranes using electrical impedance spectroscopy, J. Membr. Sci. 425 (2013) 89–97.
[27] L.N. Sim, Z.J. Wang, J. Gu, H.G.L. Coster, A.G. Fane, Detection of reverse osmosis membrane fouling with silica, bovine serum albumin and their mixture using in-situ electrical impedance spectroscopy, J. Membr. Sci. 443 (2013) 45–53.
[28] Z. Hu, A. Antony, G. Leslie, P. Le-Clech, Real-time monitoring of scale formation in reverse osmosis using electrical impedance spectroscopy, J. Membr. Sci. 453 (2014) 320–327.
[29] J. Cen, M. Vukas, G. Barton, J. Kavanagh, H.G.L. Coster, Real time fouling monitoring with electrical impedance spectroscopy, J. Membr. Sci. 484 (2015) 133–139.
[30] A. Zhu, F. Long, X. Wang, W. Zhu, J. Ma, The negative rejection of H+ in Nf of carbonate solution and its influences on membrane performance, Chemosphere 67 (2007) 1558–1565.
[31] K. Asaka, Dielectric properties of cellulose acetate reverse osmosis membranes in aqueous salt solutions, J. Membr. Sci. 50 (1990) 71–84.
[32] J.M. Kavanagh, S. Hussain, T.C. Chilcott, H.G.L. Coster, Fouling of reverse osmosis membranes using electrical impedance spectroscopy: measurements and simulations, Desalination 236 (2009) 187–193.
[33] T. Hanai, K. Zhao, K. Asaka, K. Asami, Dielectric theory of concentration polarization. Relaxation of capacitance and conductance for electrolyte solutions with locally varying conductivity, J. Membr. Sci. 64 (1991) 153–161.
[34] T. Osaki, A. Tanioka, Dielectric relaxation on the intermediate layer in a bipolar membrane under the water splitting phenomenon: Ii. double dielectric relaxation and identification of phase parameters, J. Colloid Interface Sci. 253 (2002) 94–102.
[35] Z. Zhang, V.M. Bright, A.R. Greenberg, Use of capacitive microsensors and ultrasonic time-domain reflectometry for in-situ quantification of concentration polarization and membrane fouling in pressure-driven membrane filtration, Sens. Actuators B: Chem. 117 (2006) 323–331.
[36] Ś.F. Boerlage, M.D. Kennedy, I. Bremere, G.J. Witkamp, J.P. van der Hoek, J. C. Schippers, Stable barium sulphate supersaturation in reverse osmosis, J. Membr. Sci. 179 (2000) 53–68.
[37] C.-J. Lin, S. Shirazi, P. Rao, Mechanistic model for Ca So 4 fouling on nanofiltration membrane, J. Environ. Eng. 131 (2005) 1387–1392.
[38] T. Hanai, H. Zhang, K. Sekine, K. Asaka, K. Asami, The number of interfaces and the associated dielectric relaxations in heterogeneous systems, Ferroelectrics 86 (1988) 191–204.
[39] M.T. Darestani, T.C. Chilcott, H.G.L. Coster, Electrical impedance spectroscopy study of piezoelectric Pvdf membranes, J. Solid State Electrochem. 18 (2014) 595–605.
[40] V.V.R. Nandigana, N.R. Aluru, Characterization of electrochemical properties of a micro-nanochannel integrated system using computational impedance spectroscopy (Cis), Electrochim. Acta 105 (2013) 514–523.
[41] M.J. Ariza, A. Canas, J. Benavente, Electrokinetic and electrochemical characterizations of porous membranes, Colloids Surf. a – Physicochem. Eng. Asp. 189 (2001) 247–256.
[42] P.K. Sow, D. Parvatalu, A. Bhardwaj, B.N. Prabhu, A.N. Bhaskarwar, A. Shukla, Impedance spectroscopic determination of effect of temperature on the transport resistances of an electro-electrodialysis cell used for concentration of hydriodic acid, J. Appl. Electrochem. 43 (2013) 31–41.
[43] A.S. Bauskar, C.A. Rice, Impact of anode catalyst layer porosity on the performance of a direct formic acid fuel cell, Electrochim. Acta 62 (2012) 36–41.
[44] J.-B. Jorcin, M.E. Orazem, N. Pébère, B. Tribollet, Cpe analysis by local electrochemical impedance spectroscopy, Electrochim. Acta 51 (2006) 1473–1479.
[45] C. Hsu, F. Mansfeld, Technical note: concerning the conversion of the constant phase element parameter Y0 into a capacitance, Corrosion 57 (2001) 747–748.